RESEARCH ARTICLE
SPACE PHYSICS: IONOSPHERIC PHYSICS

Earth and Planetary Physics
9: 980–987, 2025
doi: 10.26464/epp2025019

Morphology and dynamics of sporadic E layers observed by amateur radio

WenYu Hao[1], Tao Yu[1]*, Yang-Yi Sun[1], Jin Wang[1], and LiHui Qiu[2]

[1]School of Geophysics & Geomatics, China University of Geosciences, Wuhan 430074, China;

[2]International Research Center for Space and Planetary Environmental Science (i-SPES), Kyushu University, Fukuoka 8190395, Japan

Key Points:

- We investigated the E_s layer by analyzing amateur radio data.
- The horizontal structure of the E_s layer mainly elongates in an east–west direction.
- The E_s layer shows a northeast–southwest movement at speeds of 50–200 m/s.

Citation: Hao, W. Y., Yu, T., Sun, Y.-Y., Wang, J., and Qiu, L. H. (2025). Morphology and dynamics of sporadic E layers observed by amateur radio. *Earth Planet. Phys.*, *9*(4), 980–987. http://doi.org/10.26464/epp2025019

Abstract: The E_s layer is a thin layer that concentrates metallic ions in the mesosphere and lower thermosphere (MLT) region. When it occurs, it can affect the performance of the Global Navigation Satellite System and high/very high frequency (HF/VHF) radio communications. Previous studies mainly focused on the one-dimensional structure of E_s layer in the vertical direction. However, due to the limitation of observations, the horizontal structure of E_s layers is not yet fully understood. This study investigated the horizontal structure of E_s layers using amateur radio data in the European sector during the summer of 2020. Statistical analysis shows that the horizontal structure of E_s layer is mainly elongated in the east–west direction. In addition, we investigated the dynamics of the E_s layers, which primarily propagates in the northeast–southwest direction with a speed of 50–200 m/s. The results provide us a way for obtaining the horizontal structure and dynamic features of E_s layers, which can help improve our understanding of the formation and evolution of E_s layers.

Keywords: amateur radio reporting networks; sporadic E layer; horizontal structure; wind shear; dynamic feature

1. Introduction

Sporadic E (E_s) layers are thin layers of high electron density in the mesosphere–lower thermosphere (MLT) region (e.g., Smith, 1978; Whitehead, 1989; Mathews et al., 1993; Johnson and Killeen, 1995; Mathews, 1998; Haldoupis, 2011; Vincent, 2015). They appear occasionally at altitudes of ~100 km (e.g., Smith, 1957; Smith and Mechtly, 1972; Haldoupis et al., 2007; Haldoupis, 2011) and typically have a horizontal extent of between 10 km and a few hundred km (From and Whitehead, 1978; Maeda and Heki, 2014; Sun WJ et al., 2021). Previous studies show that the E_s layers can interfere with high-frequency (HF) communication, radar and communication systems at Ultra High Frequency (UHF), and satellite radio signal scintillation (Miya et al., 1978; Miya, 1996; Smith and Igarashi, 1997; Yeh et al., 2012; Yue XN et al., 2016; Sakai et al., 2020; Hosokawa et al., 2021).

Traditionally, E_s layers are mainly monitored through ionosondes, rockets, incoherent scatter radar (ISR), GNSS satellite radio occultation (RO), and GNSS receivers. ISR captures the detailed structure and evolution of E_s layers (e.g., Smith, 1978; Christakis et al., 2009; Haldoupis, 2011), but ISR observations are rare. Rockets can provide in situ measurements of ion and electron concentration (e.g., Smith and Mechtly, 1972; Kopp, 1997; Grebowsky and Bilitza, 2000), but their launches are restricted in time and location, and also very expensive. Ionosondes are cost-effective and can monitor the evolution of E_s layers continuously (e.g., Baggaley, 1985; Haldoupis et al., 2006; Reinisch and Galkin, 2011; Sun WJ et al., 2018; Qiu LH et al., 2021; Wang J et al., 2021; Sun YY et al., 2025). However, their distribution is limited primarily to the ocean and desert areas. Radio occultation (RO) observations can be used to study the global distribution and seasonal variations of E_s layers (e. g., Arras et al., 2008; Yeh et al., 2012; Arras and Wickert, 2018; Tsai et al., 2018; Qiu LH et al., 2019; Yamazaki et al., 2022), but could not obtain the time evolution or structure of E_s layers continuously over a region.

At present, many investigators study the horizontal structure of E_s layers over Asia by using the GNSS receiver network (e. g., Maeda and Heki, 2014, 2015; Sun WJ et al., 2018, 2021; Saito et al., 2021). Maeda and Heki (2014), for the first time, presented one E_s layer observed by GNSS over Japan. Maeda and Heki (2015) then analyzed the statistical characteristics of the E_s layer structure, which mainly elongate in the NE-SW direction and move to SW and NW at speeds of 30–100 m/s. By analyzing the GNSS TEC over

First author: W. Y. Hao, Wenyhao@foxmail.com
Correspondence to: T. Yu, yutaommnn@163.com
Received 14 JAN 2025; Accepted 23 JAN 2025.
First Published online 13 MAR 2025.

China, Sun WJ et al. (2018) also showed that the E_s layers elongate in the NW-SE direction, along with SW and NE movement at speeds of 50–200 m/s. The E_s layer structure is very large, more than 1000 km in width.

Recently, because of its wide geographical and temporal coverage, amateur ham radio data has provided a new approach to exploring ionospheric phenomena (e. g., Rice et al., 2011; Frissell et al., 2014, 2018, 2019, 2022; Deacon et al., 2019, 2021, 2022). By analyzing amateur ham radio data, Deacon et al. (2022) proposed a new way of observing E_s layers, and presented two instances of E_s layers over Europe for over an hour, subsequently merging and then slowly dispersing.

In this study, using the method proposed by Deacon et al. (2022), we investigated the horizontal structure of E_s layers by amateur radio data in 2020 over the Europa region. Furthermore, the movement characteristics of E_s layers are also statistically analyzed to show their dynamic evolution.

2. Data and Methodology

In this study, amateur radio data is observed by the Weak Signal Propagation Reporter Network (WSPRnet). By using the FT8 mode communication, the WSPRnet website can monitor and log weak signals across amateur radio bands. Each data point includes the callsigns of the transmitting and receiving stations, as well as the time, frequency, station locations, and so on.

Based on the approach proposed by Deacon et al. (2022), signals transmitted by amateur radio stations within the 28–70 MHz frequency range (specifically 28, 50, and 70 MHz bands) and exhibiting communication distances between 750 km and 2500 km were identified as potential indicators of E_s layer propagation. The communication distance is selected to eliminate possible influence from the ground wave, tropospheric scatter, and multi-hop echoes. The selected signal of E_s layer could then be mapped into the midpoint location of the transmitter and receiver. Figure 1 shows the locations of transmitters (red pentagrams) and receivers (blue circles) of the amateur ham radio stations over Europe. The distribution covers the main part of Europa region and shows that it is wide enough to study the E_s layer. The black triangle represents the ionosonde stations, the name and locations of which are shown in Table 1.

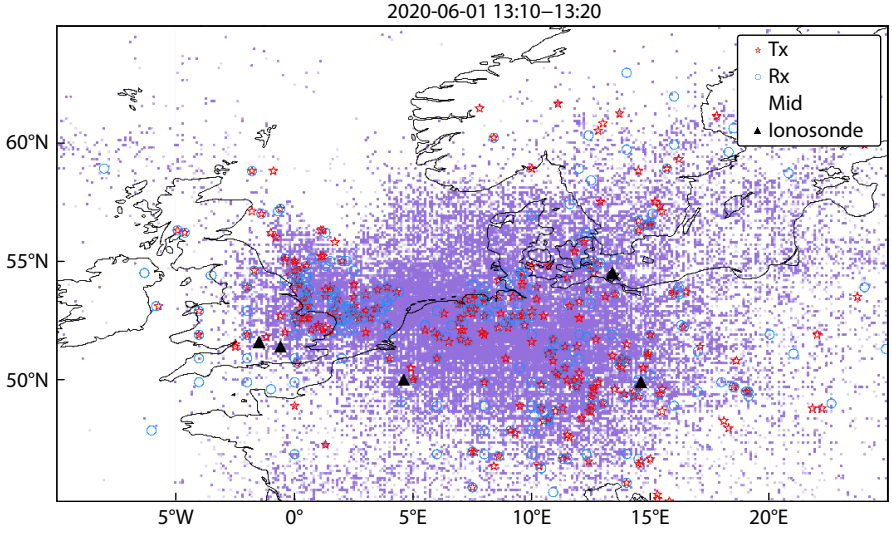

Figure 1. Amateur radio transmitting (red pentagrams) and receiving (blue circles) stations in Europe from 13:10 to 13:20 UT on June 6, 2020. The purple dots show the midpoint of the transmitter and receiver, and the black triangle represents the ionosonde station.

To verify the reliability of the method, Figure 2 shows the MUF (Maximum Usable Frequency) of the F layer and the E_s layer derived from ITU-R 1240 and ITU-R 533-8 (the f_oE is replaced by f_oEs), respectively. The critical frequency of the ionospheric F_2 layer (f_oF_2) is 7 MHz, the ratio of the maximum usable frequency at a distance of 3000 km to the f_oF_2 (M(3000)F_2) is 3.6 MHz, the height of the E_s layer (h'Es) is 110 km and the critical frequency of the E_s layer (f_oEs) is 3, 5, 6, 8 MHz, which is often observed by ionosondes (RL052, −0.6°E, 51.5°N). The results show that the communication frequency through the F layer (black line) is lower than 28 MHz (gray dash line). In other words, when the frequency is higher than 28 MHz, it is impossible to communicate by the F layer within 2500 km. When the f_oEs is higher than 6 MHz, the communication frequency from the E_s layer can be higher than 28 MHz at a distance greater than 1500 km (orange line). If f_oEs is 8 MHz, a shorter distance can support the communication of 28 MHz. The results suggested that the E_s layer signal can be identified by choosing the signal with a frequency higher than 28 MHz, and a communication distance of 750–2500 km. To further verify this method, we selected signals with a midpoint near the

Table 1. Names and exact locations of the five ionosondes.

NAME	Longitude (°E)	Latitude (°N)
JR055	13.4	54.6
FF051	−1.5	51.7
PQ052	14.6	50.0
RL052	−0.6	51.5
DB049	4.6	50.1

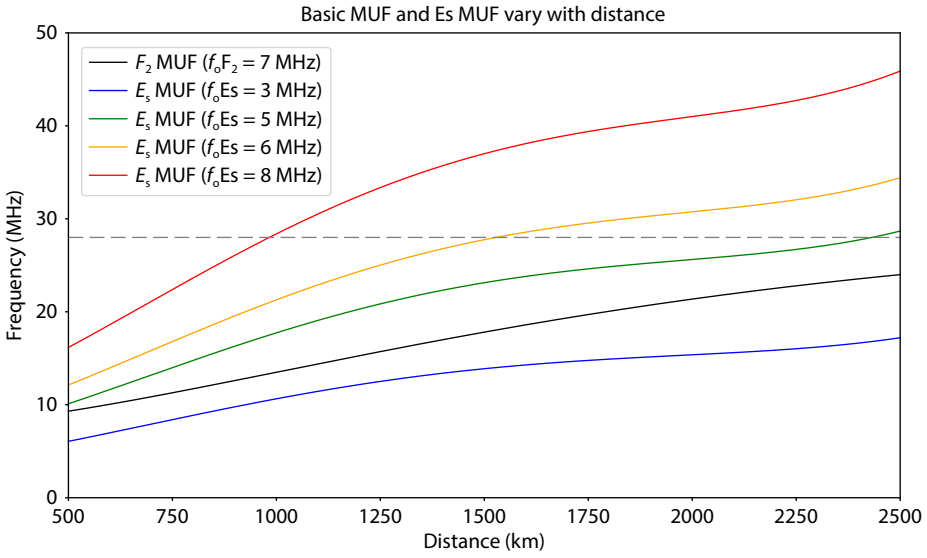

Figure 2. Maximum Usable Frequency (MUF) of *F* layer and E_s layer. MUF of *F* layer with f_oF_2 = 7 MHz is showed with black line and the MUF of E_s layer are shown with red line (f_oEs = 8 MHz), orange line (f_oEs = 6 MHz), green line (f_oEs = 5 MHz) and blue line (f_oEs = 3 MHz).

ionosonde (DB049, 4.6°E, 50.1°N) and statistically analyzed them in Table 2. The table shows the number of E_s layers observed by ionosonde with f_oEs from 3 MHz to 9 MHz (foes_num), the amount of communications supported by these E_s layers (Ham_num), and their ratio (Ham_num/foes_num). It is noted that the ratio becomes higher when the f_oEs is larger, which suggests that the dense E_s layer can support more communication than the ordinary E_s layer. Any f_oEs lower than 3 MHz is ignored.

3. Results

Figure 3 shows the E_s layer signal recorded by amateur radio and ionosondes during the period from 10:40 to 10:50 UT on June 3, 2020. The purple dots indicate the midpoints of all amateur radio frequencies, while the red dots indicate the identified E_s layer signal. The signals detected by amateur radio stations in the 28–70 MHz range (specifically 28/50/70 MHz bands) and exhibiting communication distance within 750–2500 km. Black triangles represent the ionosondes. The Figure 3 shows that the E_s layer signal occurred mainly around 55°N. It had a NE-SW elongation and had a horizontal scale of ~2000 km. Note that a strong correlation was observed between elevated f_oEs values and the spatial coincidence of intense E_s layer events with ionosonde locations, whereas stations outside these regions showed no significant enhancement. The results show that the behavior of f_oEs recorded by the ionosondes agrees with the E_s layer signal recorded by the amateur radio network.

Figure 4 shows the E_s layer indicated from the amateur radio data and the f_oEs recorded by ionosondes from 10:00 to 15:00 UT on August 8, 2020. Initially, the E_s layer signal occurred near 55°N. The ionosonde was not covered by the E_s layer signal and showed a low f_oEs value (about 4 MHz) that may not support the communication of amateur radio frequency of 28 MHz as shown in Figure 2. The E_s layer then moved southward, arriving near 50°N at 11:00 UT. During this period, the E_s layer signal reached the ionosonde that showed a higher f_oEs. Thereafter, the E_s layer signal passed over the ionosonde which had a large f_oEs value with about 8MHz at 12:00–13:00 UT. The large f_oEs can support the communication of amateur radio at 28 MHz. As the E_s layer continued to move southwest slowly, the E_s layer signal moved away from the ionosonde that had a decreased f_oEs. By 14:00 UT, the E_s layer signal had moved beyond the region observed by the ionosonde. In Figure 5, we also show the ionograms recorded during the same period. The results show that the E_s layer observed by the ionosonde became larger when it was covered by the E_s layer signal observed by the Ham data, especially during 11:00 UT to 14:00 UT.

Table 2. The number of E_s layers in 2020 observed by ionosonde (DB049) with f_oEs from 3MHz to 9MHz (foes_num), the amount of communications supported by these E_s layers (Ham_num), and their ratio (Ham_num/foes_num) in 2020.

f_oEs (MHz)	foes_num	Ham_num	Ham_num/foes_num
3	17159	16535	0.96
4	5936	21549	3.63
5	3053	28269	9.26
6	1326	21274	16.04
7	517	12949	25.05
8	337	10825	32.12
9	269	10279	38.21

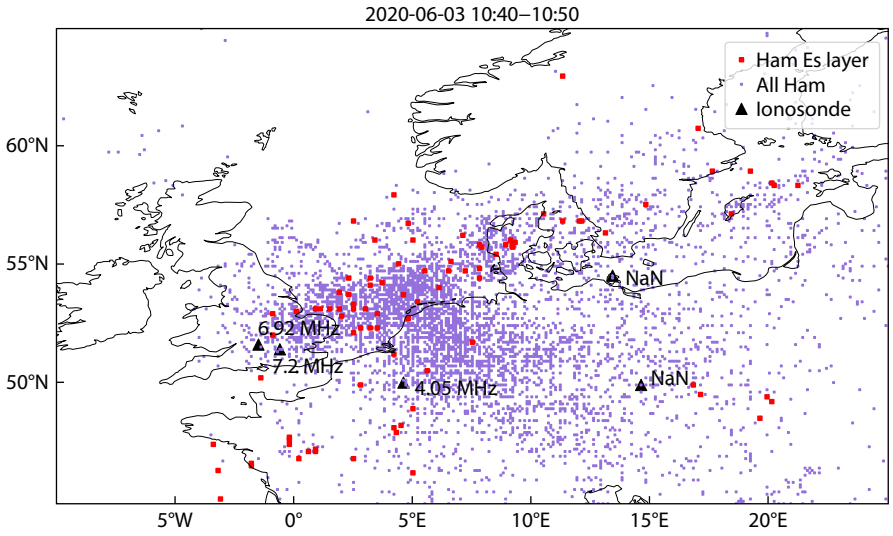

Figure 3. E_s layer indicated by amateur radio (purple and red dots) and ionosondes at 10:40–10:50 UT on June 3, 2020. The purple dots show the midpoints of all amateur radio frequencies. The red dots indicate the E_s layer signal specifically. The triangles represent the ionosondes.

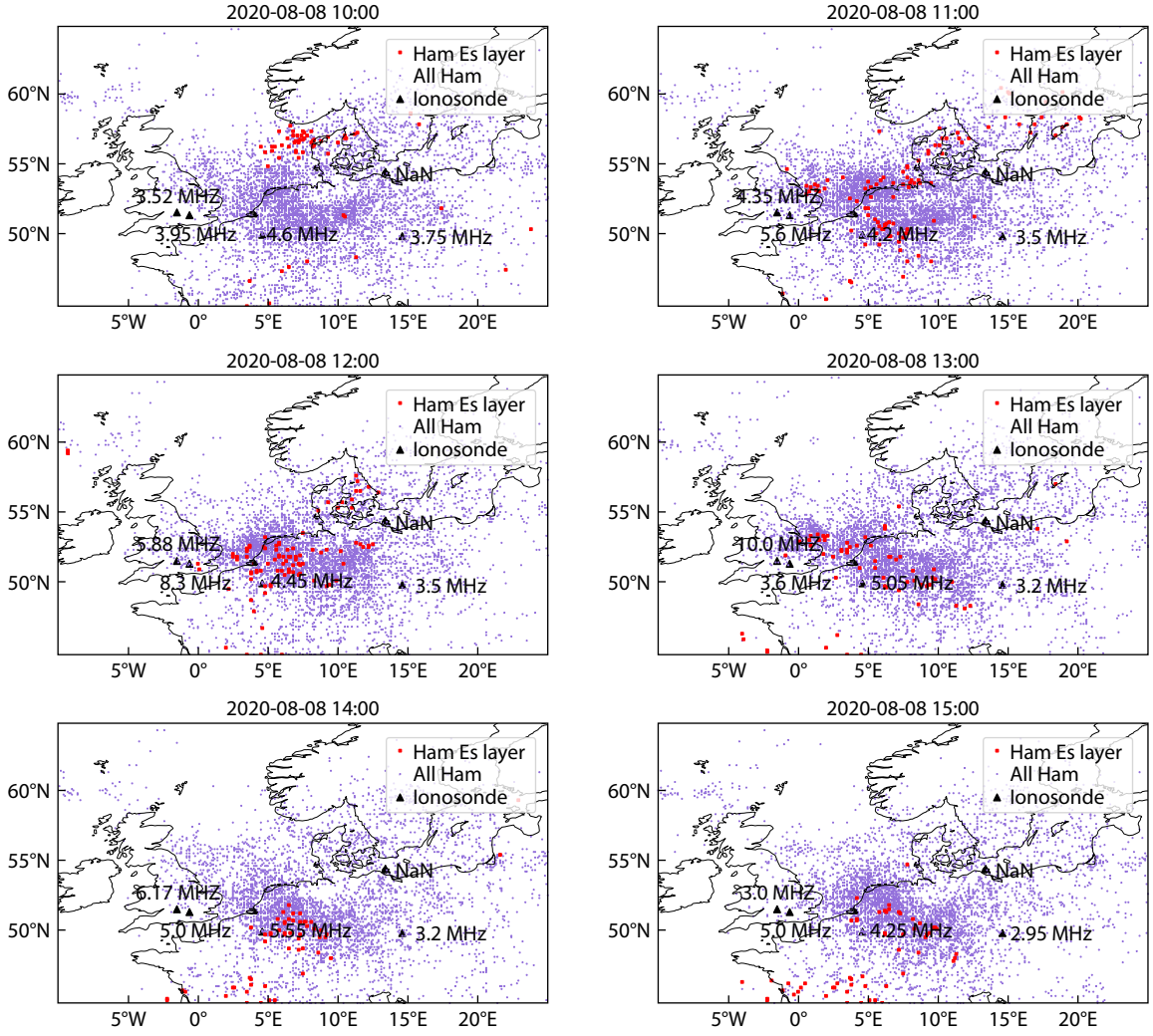

Figure 4. The evolution of E_s layer signal as indicated by the amateur radio data and its comparison with the ionosondes at 10:00–15:00 UT on August 8, 2020.

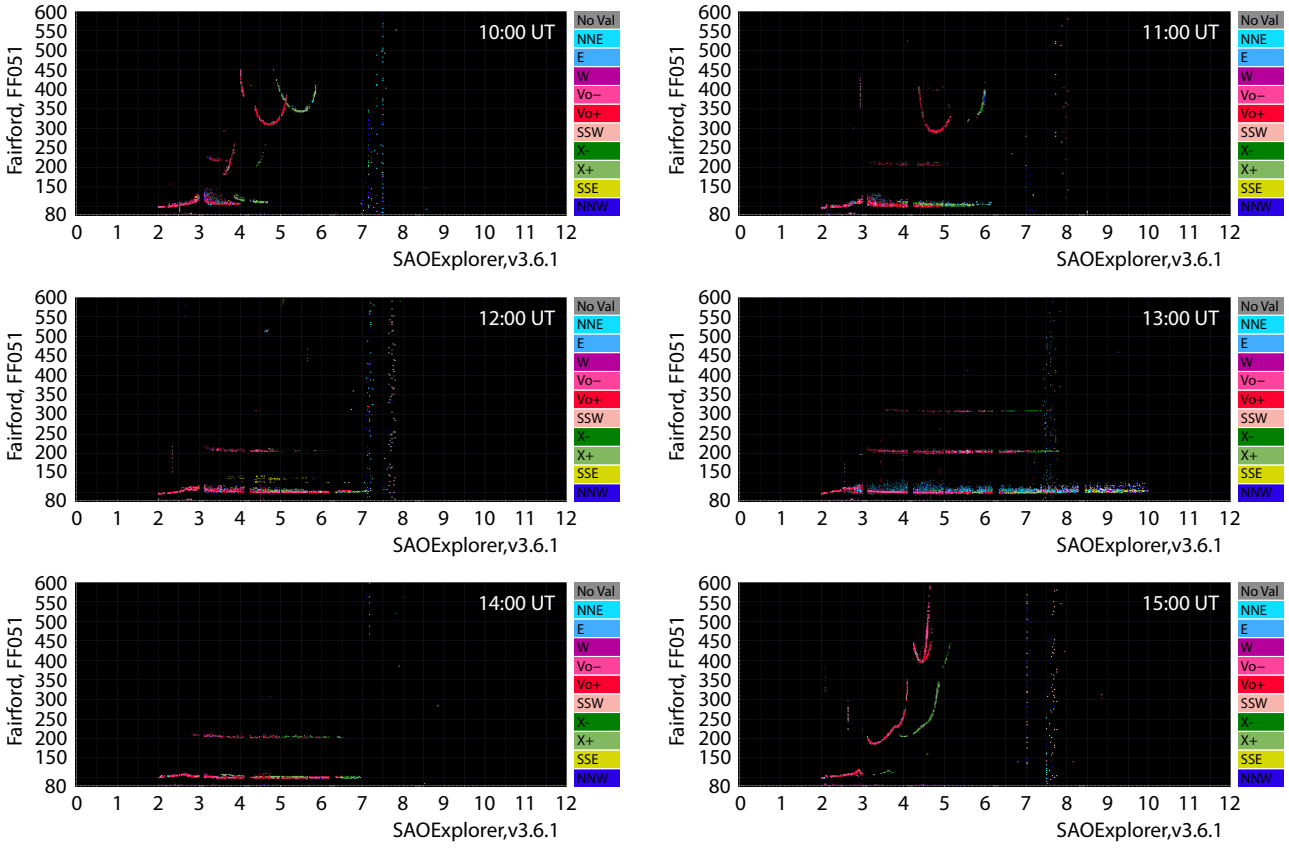

Figure 5. The ionograms recorded during 10:00–15:00 UT on August 8, 2020 in FF051 station. The horizontal axis is the frequency, and the unit is MHz. The vertical axis is the height and the unit is km.

Figure 6 presents another case study showing the behavior of E_s layer signal and f_oEs at 6:30–11:30 UT on July 19, 2020. The plot shows that the E_s layer was initially observed around 55°N, which did not overlap with the ionosonde showing a low f_oEs. At 8:30 UT, the E_s layer signal reached 50°N, covering the ionosonde that showed a higher f_oEs value (about 5–6 MHz). As the E_s layer continued to move, the ionosonde became uncovered by the E_s layer signal again and showed a decrease in f_oEs behavior. At 11:30 UT, the E_s layer moved beyond the ionosonde region.

To identify the elongation and velocity of E_s layers, a statistical analysis was performed, analyzing the 1546 cases recorded by amateur radio over Europe in 2020. We translated the centers of all E_s events to the coordinate origin, superimposed these events, and analyzed the statistical patterns of E_s extension directions and spatial distributions. We calculated the geographic centroid of all observed E_s layer occurrences within specific time intervals. By tracking the movement of this centroid over time, we were able to estimate the overall drift and velocity of the E_s layers.

The statistical results, as shown in Figure 7, illustrate that the E_s layer mainly occurred in the daytime and the summer months. The E_s layer structures were elongated primarily in the east–west direction, mainly moving southwestward at an average speed of 50–200 m/s.

4. Discussion

The statistical results show that E_s layer structures comprise two main types. In one case, the E_s layer structure could be elongated in a NE-SW direction, which mainly agrees with previous E_s layer behavior recorded by the GNSS observation network in Japan (Maeda and Heki, 2015). On the other hand, the E_s layer structures could be elongated in a NW-SE direction, which agrees with the observations of Sun WJ et al. (2021).

Note that the structure of the E_s layer observed by amateur radio as shown in the study is wider than that recorded by GNSS, which is a rather narrow band layer. GNSS can mainly identify dense E_s layer (f_oEs $\geq$ 14 MHz), whereas amateur radio's ability to identify the much weaker E_s layer signal (f_oEs $\geq$ 6 MHz) may contribute to the difference.

The wind-shear theory proposed by Whitehead (1961) is the main formation mechanism used to describe the mid-latitude E_s layer formation. The wind shear theory has been well confirmed by observations and simulations (e.g., Yuan T et al., 2014; Cai X et al., 2019; Qiu LH et al., 2019; Yu BK et al., 2019; Yamazaki et al., 2022). By analyzing the horizontal structure of the ion convergence region (HSICR) from the Whole Atmosphere Community Climate Model with thermosphere and ionosphere eXtension (WACCM-X 2.1), Qiu LH et al. (2023a) suggested that the E_s layer structure could have a NE-SW or NW-SE elongation. The HSICR is also wider than the E_s layer observed by the GNSS network, which agrees with the E_s layer structure identified from the amateur radio data in the present study. On the other hand, the E_s layer behaving as a NE-SW elongation shows a southwest movement at a speed of

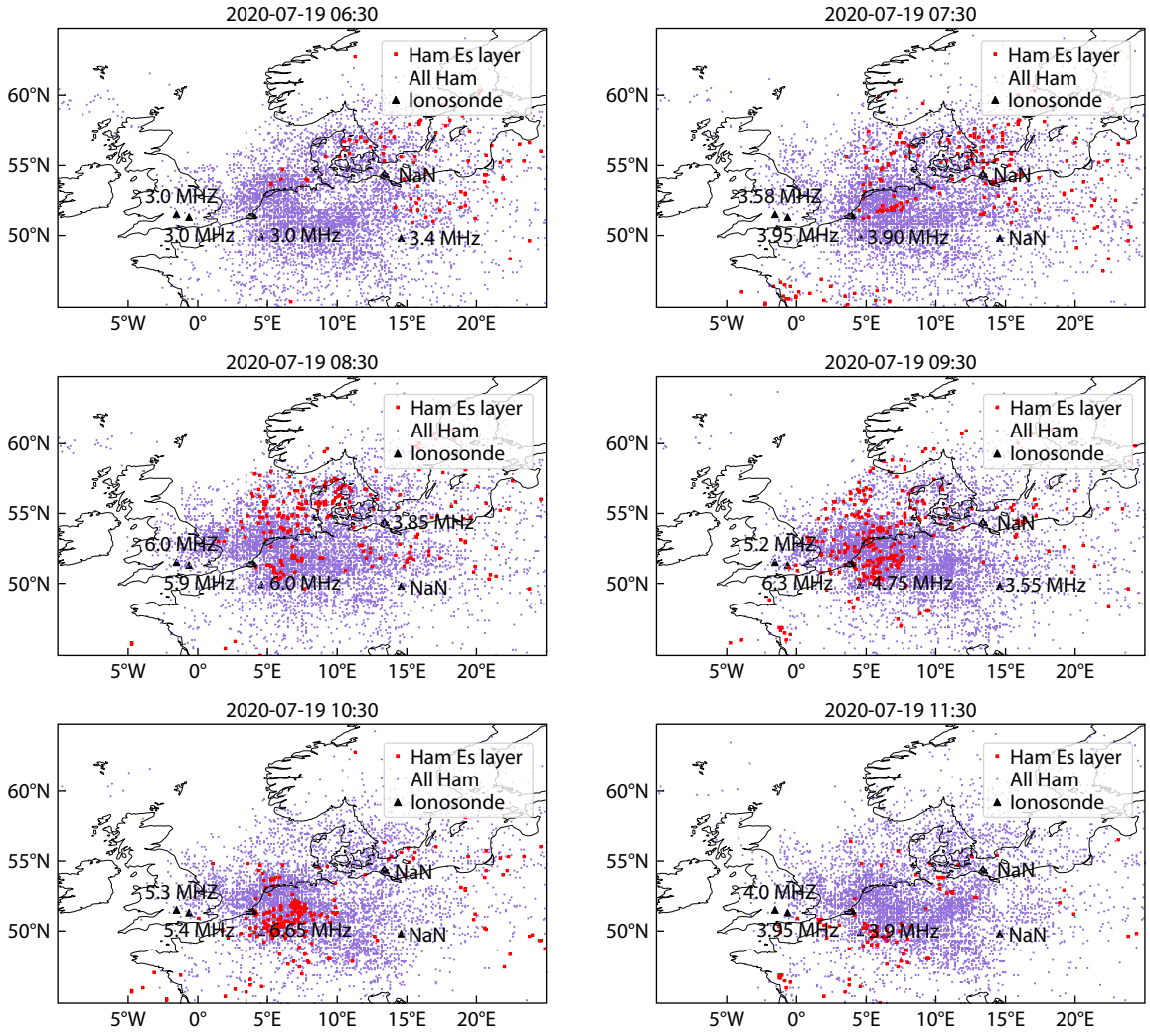

Figure 6. Same as Figure 4, but for the case at 6:30–11:30 UT on July 19, 2020.

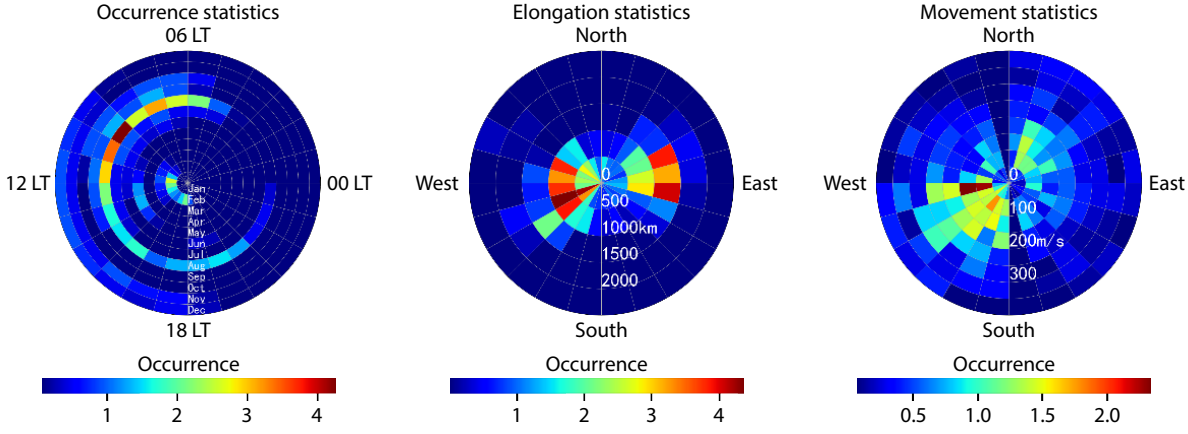

Figure 7. Statistical analysis of E_s layers over Europe in 2020 based on amateur radio data. The left panel shows the temporal distribution of E_s layer occurrences. The radial axis represents the months of the year, while the azimuthal axis represents the local time. The color scale indicates the percentage of the E_s layer occurrences relative to the total observed events. The middle panel shows the statistical result of elongation and azimuth of the E_s layer. The radial axis represents the extent of elongation in kilometers, while the azimuthal axis indicates the direction of elongation. The color intensity corresponds to the percentage of observations with specific elongation characteristics. The right panel shows the distributions of speed and movement direction. The radial axis represents the velocity of movement in meters per second, while the azimuthal axis indicates the direction of movement. The color scale reflects the percentage of observations with particular movement characteristics.

50–200 m/s (Figure 6). This also agrees with the results presented by Sun WJ et al. (2021), which showed that the E_s layer has a speed of 30–210 m/s. However, Maeda and Heki (2015) suggested that the drift direction of the E_s layer is mainly SW and NW with a speed of 30–100 m/s. As for the physics of the E_s layer movement, previous studies have confirmed that the vertical movement of the E_s layer is mainly controlled by the descent of wind shear node controlled by atmospheric waves (Haldoupis, 2011; Qiu LH et al., 2021, 2023b, 2023c; Andoh et al., 2022, 2023; Yu Y et al., 2023). In the horizontal direction, the movement of the E_s layer maybe also controlled by the horizontal variations of the wind shear node, which should be examined in the future.

5. Conclusion

In this study, we investigated the horizontal structure of E_s layer by analyzing amateur radio data over Europe in 2020. Subsequent statistical analysis of E_s layer signal showed that the horizontal structure of the E_s layer mainly elongates in an east–west direction. The E_s layer is not stationary, and shows a northeast–southwest movement at speeds of 50–200 m/s. The results captured the horizontal structure and dynamics evolution of E_s layer, which also suggests that amateur radio data can serve as an effective method for studying the E_s layer morphology and behavior. The studies of the dynamics of the E_s layer may be helpful for early warnings of ionospheric disturbances affecting HF/VHF radio communications and radar operations..

Acknowledgments

The research is supported by the National Natural Science Foundation of China (42230207, 42104165). We are especially grateful to the wsprnet.org for providing amateur radio data. The authors acknowledge the use of ionospheric data from the USAF NEXION Digisonde network.

References

Andoh, S., Saito, A., and Shinagawa, H. (2022). Numerical simulations on day-to-day variations of low-latitude Es layers at Arecibo. *Geophys. Res. Lett.*, *49*(7), e2021GL097473. https://doi.org/10.1029/2021GL097473

Andoh, S., Saito, A., and Shinagawa, H. (2023). Simulation of horizontal sporadic E layer movement driven by atmospheric tides. *Earth Planets Space*, *75*(1), 86. https://doi.org/10.1186/s40623-023-01837-0

Arras, C., Wickert, J., Beyerle, G., Heise, S., Schmidt, T., and Jacobi, C. (2008). A global climatology of ionospheric irregularities derived from GPS radio occultation. *Geophys. Res. Lett.*, *35*(14), L14809. https://doi.org/10.1029/2008GL034158

Arras, C., and Wickert, J. (2018). Estimation of ionospheric sporadic E intensities from GPS radio occultation measurements. *J. Atmos. Sol.-Terr. Phys.*, *171*, 60–63. https://doi.org/10.1016/j.jastp.2017.08.006

Baggaley, W. J. (1985). Seasonal characteristics of daytime E_s occurrence in the southern hemisphere. *J. Atmos. Terr. Phys.*, *47*(6), 611–614. https://doi.org/10.1016/0021-9169(85)90044-3

Cai, X., Yuan, T., Eccles, J. V., and Raizada, S. (2019). Investigation on the distinct nocturnal secondary sodium layer behavior above 95 km in winter and summer over Logan, UT (41.7°N, 112°W) and Arecibo Observatory, PR (18.3°N, 67°W). *J. Geophys. Res.: Space Phys.*, *124*(11), 9610–9625. https://doi.org/10.1029/2019JA026746

Christakis, N., Haldoupis, C., Zhou, Q., and Meek, C. (2009). Seasonal variability and descent of mid-latitude sporadic E layers at Arecibo. *Ann. Geophys.*, *27*(3), 923–931. https://doi.org/10.5194/angeo-27-923-2009

Deacon, C., Mitchell, C., and Witvliet, B. A. (2019). Investigation of the polarization of 50 MHz signals via Sporadic-E reflection. In *Proceedings of the Nordic HF Conference*. Fårö, Sweden: Nordic Radio Society NRS.

Deacon, C., Mitchell, C., and Watson, R. (2022). Consolidated amateur radio signal reports as indicators of intense sporadic E layers. *Atmosphere*, *13*(6), 906. https://doi.org/10.3390/atmos13060906

Deacon, C. J., Witvliet, B. A., Steendam, S. N., and Mitchell, C. N. (2021). Rapid and accurate measurement of polarization and fading of weak VHF signals obliquely reflected from sporadic-E Layers. *IEEE Trans. Antenn. Propag.*, *69*(7), 4033–4048. https://doi.org/10.1109/TAP.2020.3044654

Frissell, N. A., Miller, E. S., Kaeppler, S. R., Ceglia, F., Pascoe, D., Sinanis, N., Smith, P., Williams, R., and Shovkoplyas, A. (2014). Ionospheric sounding using real-time amateur radio reporting networks. *Space Weather*, *12*(12), 651–656. https://doi.org/10.1002/2014SW001132

Frissell, N. A., Katz, J. D., Gunning, S. W., Vega, J. S., Gerrard, A. J., Earle, G. D., Moses, M. L., West, M. L., Huba, J. D., … Silver, H. W. (2018). Modeling amateur radio soundings of the ionospheric response to the 2017 Great American Eclipse. *Geophys. Res. Lett.*, *45*(10), 4665–4674. https://doi.org/10.1029/2018GL077324

Frissell, N. A., Vega, J. S., Markowitz, E., Gerrard, A. J., Engelke, W. D., Erickson, P. J., Miller, E. S., Luetzelschwab, R. C., and Bortnik, J. (2019). High-frequency communications response to solar activity in September 2017 as observed by amateur radio networks. *Space Wea.*, *17*(1), 118–132. https://doi.org/10.1029/2018SW002008

Frissell, N. A., Kaeppler, S. R., Sanchez, D. F., Perry, G. W., Engelke, W. D., Erickson, P. J., Coster, A. J., Ruohoniemi, J. M., Baker, J. B. H., and West, M. L. (2022). First observations of large scale traveling ionospheric disturbances using automated amateur radio receiving networks. *Geophys. Res. Lett.*, *49*(5), e2022GL097879. https://doi.org/10.1029/2022GL097879

From, W. R., and Whitehead, J. D. (1978). On the peculiar shape of sporadic-*E* clouds. *J. Atmos. Terr. Phys.*, *40*(9), 1025–1028. https://doi.org/10.1016/0021-9169(78)90006-5

Grebowsky, J. M., and Bilitza, D. (2000). Sounding rocket data base of E- and D-region ion composition. *Adv. Space Res.*, *25*(1), 183–192. https://doi.org/10.1016/S0273-1177(99)00916-3

Haldoupis, C., Meek, C., Christakis, N., Pancheva, D., and Bourdillon, A. (2006). Ionogram height–time–intensity observations of descending sporadic *E* layers at mid-latitude. *J. Atmos. Sol.-Terr. Phys.*, *68*(3-5), 539–557. https://doi.org/10.1016/j.jastp.2005.03.020

Haldoupis, C., Pancheva, D., Singer, W., Meek, C., and MacDougall, J. (2007). An explanation for the seasonal dependence of midlatitude sporadic *E* layers. *J. Geophys. Res.: Space Phys.*, *112*(A6), A06315. https://doi.org/10.1029/2007JA012322

Haldoupis, C. (2011). A tutorial review on sporadic *E* layers. In M. A. Abdu, et al. (Eds.), *Aeronomy of the Earth's Atmosphere and Ionosphere* (pp. 381–394). Dordrecht: Springer. https://doi.org/10.1007/978-94-007-0326-1_29

Hosokawa, K., Kimura, K., Sakai, J., Saito, S., Tomizawa, I., Nishioka, M., Tsugawa, T., and Ishii, M. (2021). Visualizing sporadic E using aeronautical navigation signals at VHF frequencies. *J. Space Wea. Space Clim.*, *11*(6), 6. https://doi.org/10.1051/swsc/2020075

Johnson, R. M., and Killeen, T. L. (1995). *The Upper Mesosphere and Lower Thermosphere: A Review of Experiment and Theory*. Washington: American Geophysical Union. https://doi.org/10.1029/GM087

Kopp, E. (1997). On the abundance of metal ions in the lower ionosphere. *J. Geophys. Res.: Space Phys.*, *102*(A5), 9667–9674. https://doi.org/10.1029/97JA00384

Maeda, J., and Heki, K. (2014). Two-dimensional observations of midlatitude sporadic *E* irregularities with a dense GPS array in Japan. *Radio Sci.*, *49*(1), 28–35. https://doi.org/10.1002/2013RS005295

Maeda, J., and Heki, K. (2015). Morphology and dynamics of daytime mid-latitude sporadic-E patches revealed by GPS total electron content observations in Japan. *Earth Planets Space*, *67*(1), 89. https://doi.org/10.1186/s40623-015-0257-4

Mathews, J. D., Zhou, Q., Philbrick, C. R., Morton, Y. T., and Gardner, C. S. (1993). Observations of ion and sodium layer coupled processes during AIDA. *J. Atmos. Terr. Phys.*, *55*(3), 487–498. https://doi.org/10.1016/0021-9169(93)

90083-B

Mathews, J. D. (1998). Sporadic E: Current views and recent progress. *J. Atmos. Sol.-Terr. Phys.*, *60*(4), 413–435. https://doi.org/10.1016/S1364-6826(97)00043-6

Miya, K., Shimizu, K., and Kojima, T. (1978). Oblique-incidence sporadic-*E* propagation and its ionospheric attenuation. *Radio Sci.*, *13*(3), 559–570. https://doi.org/10.1029/RS013i003p00559

Miya, K. (1996). My memory of efforts in developing CCIR Recommendation 534-3: Method for calculating sporadic-E field strength. *IEEE Antenn. Propag. Mag.*, *38*(5), 90–93. https://doi.org/10.1109/74.544406

Qiu, L. H., Zuo, X. M., Yu, T., Sun, Y. Y., and Qi, Y. F. (2019). Comparison of global morphologies of vertical ion convergence and sporadic E occurrence rate. *Adv. Space Res.*, *63*(11), 3606–3611. https://doi.org/10.1016/j.asr.2019.02.024

Qiu, L. H., Zuo, X. M., Yu, T., Sun, Y. Y., Liu, H. X., Sun, L. F., and Zhao, B. Q. (2021). The characteristics of summer descending sporadic E layer observed with the ionosondes in the China Region. *J. Geophys. Res.: Space Phys.*, *126*(3), e2020JA028729. https://doi.org/10.1029/2020JA028729

Qiu, L. H., Lu, X., Yu, T., Yamazaki, Y., Liu, H. X., Sun, Y. Y., Wu, H. N., Zuo, X. M., Yan, X. X., … Qi, Y. F. (2023a). Horizontal structure of convergent wind shear associated with sporadic E layers over East Asia. *Earth Planet. Phys.*, *7*(5), 548–557. https://doi.org/10.26464/epp2023071

Qiu, L. H., Yamazaki, Y., Yu, T., Miyoshi, Y., and Zuo, X. M. (2023b). Numerical investigation on the height and intensity variations of sporadic E layers at mid-latitude. *J. Geophys. Res.: Space Phys.*, *128*(9), e2023JA031508. https://doi.org/10.1029/2023JA031508

Qiu, L. H., Yamazaki, Y., Yu, T., Becker, E., Miyoshi, Y., Qi, Y. F, Siddiqui, T. A., Stolle, C., Feng, W. H., … Liu, H. X. (2023c). Numerical simulations of metallic ion density perturbations in sporadic E layers caused by gravity waves. *Earth Space Sci.*, *10*(8), e2023EA003030. https://doi.org/10.1029/2023EA003030

Reinisch, B. W., and Galkin, I. A. (2011). Global ionospheric radio observatory (GIRO). *Earth Planets Space*, *63*(4), 377–381. https://doi.org/10.5047/eps.2011.03.001

Rice, D. D., Sojka, J. J., Eccles, J. V., Raitt, J. W., Brady, J. J., and Hunsucker, R. D. (2011). First results of mapping sporadic *E* with a passive observing network. *Space Wea.*, *9*(12), S12001. https://doi.org/10.1029/2011SW000678

Saito, S., Hosokawa, K., Sakai, J., and Tomizawa, I. (2021). Study of structures of the sporadic E layer by using dense GNSS network observations. *Navigation*, *68*(4), 751–758. https://doi.org/10.1002/navi.454

Sakai, J., Saito, S., Hosokawa, K., and Tomizawa, I. (2020). Anomalous propagation of radio waves from distant ILS localizers due to ionospheric sporadic-E. *Space Wea.*, *18*(8), e2020SW002517. https://doi.org/10.1029/2020SW002517

Smith, E. K., and Igarashi, K. (1997) . VHF sporadic E-a significant factor for EMI. 1997 Proceedings of International Symposium on Electromagnetic Compatibility, Beijing, China, 1997, pp. 29–32. https://doi.org/10.1109/ELMAGC.1997.617067

Smith, E. K. (1978). Temperate zone sporadic-*E* maps (f_0E_s > 7 MHz). *Radio Sci.*, *13*(3), 571–575. https://doi.org/10.1029/RS013i003p00571

Smith, E. K. Jr. (1957). *Worldwide Occurrence of Sporadic E* (pp. 178–183). Washington: US Department of Commerce, National Bureau of Standards.

Smith, L. G., and Mechtly, E. A. (1972). Rocket observations of sporadic-*E* layers. *Radio Sci.*, *7*(3), 367–376. https://doi.org/10.1029/RS007i003p00367

Sun, W. J., Ning, B. Q., Yue, X. N., Li, G. Z., Hu, L. H., Chang, S. M., Lan, J. P., Zhu, Z. P., Zhao, B. Q., and Lin, J. (2018). Strong sporadic *E* occurrence detected by ground-based GNSS. *J. Geophys. Res.: Space Phys.*, *123*(4), 3050–3062. https://doi.org/10.1002/2017JA025133

Sun, W. J., Zhao, X. K., Hu, L. H., Yang, S. P., Xie, H. Y., Chang, S. M., Ning, B. Q., Li, J. Y., Liu, L. B., and Li, G. Z. (2021). Morphological characteristics of thousand-kilometer-scale E_s structures over China. *J. Geophys. Res.: Space Phys.*, *126*(2), e2020JA028712. https://doi.org/10.1029/2020JA028712

Sun, Y. Y., Yu, T., Wang, J., and Long, C. (2025). Sporadic *E* responds to the 2022 Tonga volcano eruptions recorded by the Meridian Project. *Earth Planet. Phys.*, *9*(1), 20–28. https://doi.org/10.26464/epp2024051

Tsai, L. C., Su, S. Y., Liu, C. H., Schuh, H., Wickert, J., and Alizadeh, M. M. (2018). Global morphology of ionospheric sporadic E layer from the FormoSat-3/COSMIC GPS radio occultation experiment. *GPS Solut.*, *22*(4), 118. https://doi.org/10.1007/s10291-018-0782-2

Vincent, R. A. (2015). The dynamics of the mesosphere and lower thermosphere: a brief review. *Prog. Earth Planet. Sci.*, *2*(1), 4. https://doi.org/10.1186/s40645-015-0035-8

Wang, J., Zuo, X. M., Sun, Y. Y., Yu, T., Wang, Y. G., Qiu, L. H., Mao, T., Yan, X. X., Yang, N., … Zhao, B. Q. (2021). Multilayered sporadic-*E* response to the annular solar eclipse on June 21, 2020. *Space Wea., 19*(3), e2020SW002643. https://doi.org/10.1029/2020SW002643

Whitehead, J. D. (1961). The formation of the sporadic-E layer in the temperate zones. *J. Atmos. Terr. Phys.*, *20*(1), 49–58. https://doi.org/10.1016/0021-9169(61)90097-6

Whitehead, J. D. (1989). Recent work on mid-latitude and equatorial sporadic-*E*. *J. Atmos. Terr. Phys.*, *51*(5), 401–424. https://doi.org/10.1016/0021-9169(89)90122-0

Yamazaki, Y., Arras, C., Andoh, S., Miyoshi, Y., Shinagawa, H., Harding, B. J., Englert, C. R., Immel, T. J., Sobhkhiz-Miandehi, S., and Stolle, C. (2022). Examining the wind shear theory of sporadic E with ICON/MIGHTI winds and COSMIC-2 Radio 2 occultation data. *Geophys. Res. Lett.*, *49*(1), e2021GL096202. https://doi.org/10.1029/2021GL096202

Yeh, W. H., Huang, C. Y., Hsiao, T. Y., Chiu, T. C., Lin, C. H., and Liou, Y. A. (2012). Amplitude morphology of GPS radio occultation data for sporadic-*E* layers. *J. Geophys. Res.: Space Phys.*, *117*(A11), A11304. https://doi.org/10.1029/2012JA017875

Yu, B. K., Xue, X. H., Yue, X., Yang, C. Y., Yu, C., Dou, X. K., Ning, B. Q., and Hu, L. H. (2019). The global climatology of the intensity of the ionospheric sporadic *E* layer. *Atmos. Chem. Phys.*, *19*(6), 4139–4151. https://doi.org/10.5194/acp-19-4139-2019

Yu, Y., Yu, T., Qiu, L. H., Yan, X. X., Wang, J., Liang, Y., Liu, S., and Qi, Y. F. (2023). Comparison of the heights of sporadic E layers and vertical ion convergence parameters. *Remote Sens.*, *15*(24), 5674. https://doi.org/10.3390/rs15245674

Yuan, T., Wang, J. H., Cai, X. G., Sojka, J., Rice, D., Oberheide, J., and Criddle, N. (2014). Investigation of the seasonal and local time variations of the high-altitude sporadic Na layer (Na_s) formation and the associated midlatitude descending *E* layer (E_s) in lower E region. *J. Geophys. Res.: Space Phys.*, *119*(7), 5985–5999. https://doi.org/10.1002/2014JA019942

Yue, X. N., Schreiner, W. S., Pedatella, N. M., and Kuo, Y. H. (2016). Characterizing GPS radio occultation loss of lock due to ionospheric weather. *Space Wea.*, *14*(4), 285–299. https://doi.org/10.1002/2015SW001340